Performance of RF Plasma Thruster for Various Magnetic Field Configurations by Permanent Magnets

IEPC-2015-412／ISTS-2015-b-412

Presented at Joint Conference of 30th International Symposium on Space Technology and Science
34th International Electric Propulsion Conference and 6th Nano-satellite Symposium,
Hyogo-Kobe, Japan
July 4 – 10, 2015

Sho Ito[1], Takahiro Nakamura[2], Hiroyuki Nishida[3] and Shunjiro Shinohara[4]
Tokyo University of Agriculture and Technology, Koganei, Tokyo, 184-8588, Japan

Abstract: In order to realize a long-lived and high-powered electric propulsion system, we have been investigating an electrodeless electric propulsion concept utilizing a RF plasma source and a magnetic nozzle. In this study, the thrust performance of the RF plasma thruster is investigated under various magnetic field configurations by changing operational conditions. From the measurements of the thrust force and the total ion flux, the thrust force, specific impulse, and plasma utilization efficiency monotonically increased with an applied RF power. The discharge mode transition points, where dramatic improvement of these performance, were found. These points were varied depending on the magnetic field configuration. In the case of same plasma flow rate, higher thrust force was obtained in the thruster with the higher magnetic flux density (290 mT) than the lower magnetic flux density (52 or 140 mT). The position of the magnetic cusp in the discharge vessel could change a propellant utilization efficiency. After the discharge mode transition, this efficiency in the case that the magnetic cusp was at the center of the RF antenna was higher than that in the case of no magnetic cusp.

Nomenclature

A_e	=	cross-sectional area of thruster exit
B_r	=	radial component of magnetic field
e	=	charge of electron
F	=	thrust force
f	=	thrust force density
g_0	=	acceleration of gravity
$I_{i,sat}$	=	ion saturation current
I_{sp}	=	specific impulse
j_θ	=	azimuthal component of current density
k_B	=	Boltzmann constant
m_n	=	mass of neutral particle
$\dot{m}$	=	injected mass flow rate
$\dot{m}_{eff}$	=	effective mass flow rate
$\dot{m}_{ing}$	=	ingested mass flow rate
P_c	=	pressure of vacuum chamber
P_{source}	=	RF power for plasma production
T_n	=	temperature of neutral particle

[1] Graduate Student, Department of Mechanical Systems Engineering, 50014643009@st.tuat.ac.jp.
[2] Ph.D., Department of Mechanical Systems Engineering, takahiro.nakamura1@gmail.com.
[3] Associate Professor, Division of Advanced Mechanical Systems Engineering, hnishida@cc.tuat.ac.jp.
[4] Professor, Division of Advanced Mechanical Systems Engineering, sshinohara@cc.tuat.ac.jp.

Δt	=	pulse width
δ	=	displacement
η_t	=	thrust efficiency
η_u	=	propellant utilization efficiency

I. Introduction

AN electrodeless plasma thruster is expected as one of the promising solutions for the problems of the lifetime (electrode's erosion and contamination) of conventional electric propulsion systems in high-powered operation. In order to realize a fully-electrodeless plasma thruster, many thruster concepts have been under-development worldwide {e.g. Variable Specific Impulse Magnetoplasma Rocket (VASIMR)[1-3], Helicon Double Layer Thruster (HDLT)[4-7], Helicon Plasma Thruster[8-13] Mini-helicon Plasma Thruster[14,15]}. In these thrusters, the plasma is produced by a radio frequency (RF) power input and exhausted by the magnetic nozzle. Many of these thrusters employ a helicon plasma source for the electrodeless plasma production. This source produces the plasma by a static magnetic field and a RF power, and can provide high-density plasma for the various size scale with a high efficiency[12]. The magnetic nozzle is one of electrodeless plasma acceleration method utilizing the diverging magnetic field. The schematic of the simple helicon plasma thruster is shown in Fig. 1. In this concept, entire process is conducted by an RF antenna and a magnetic circuit, which are located outside of the discharge vessel. Therefore, plasma does not contact with any electrodes, and neutralizer is not needed. When the plasma is exhausted from the thruster passing through the magnetic nozzle, the thermal pressure of the plasma turns into the thrust force ($F_{thermal}$ in Fig. 1) at the bottom plate of the discharge vessel. In addition, the diamagnetic electric current j_θ in the magnetic nozzle turns into the electromagnetic thrust force (Lorentz force $j_\theta \times B_r = f_{diamag}$ in Fig. 1), which acts on the magnetic circuit.

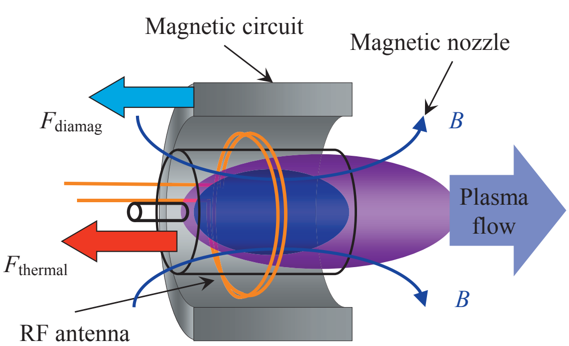

Figure 1. Schematic of simple RF plasma thruster.

The plasma acceleration in the magnetic nozzle has been investigated theoretically by Fruchtman in quasi-1-D model[16], experimentally by Takahashi[8,9], and numerically by Ahedo in 2-D computation[17]. These studies reported the plasma acceleration and the thrust production mechanism, and formulated the thrust force generation by a magnetic nozzle. In the experimental approach, Takahashi et al. separately measured the each component of the thrust force and confirmed the magnetic nozzle theory[8,9]. VASIMR group reported that the size scale and spatial location of the plasma potential structure were corresponding to the spatial distribution of the axial magnetic field gradient[18]. These previous researches indicated that the plasma pressure has to be maintained higher at the upstream of the magnetic nozzle in order to improve the thrust performance (i.e., an increment of the density peak at the center of the helicon source improves the thrust force from the magnetic nozzle). In addition, a higher magnetic flux density is needed not only to confine higher plasma pressure but also to achieve the magnetic nozzle acceleration closer to the theoretical limit in the actual thruster[9]. The VASIMR has achieved higher thrust performance (thrust force of 5.8 N and thrust efficiency of 72 %) by a combination of the high-powered helicon source (up to 30 kW) and an additional ion cyclotron resonance heating (up to170 kW), with the higher flux density magnetic nozzle (up to 2 T)[19]. However, the superconducting coil system is required for forming such a high magnetic field, which leads the thruster system being very large and complex. If the RF plasma thruster can be constructed with simple and compact components, the RF plasma thruster could be applied to wide range space missions.

The compact RF plasma thruster with simple components {RF antenna, discharge vessel, and permanent magnets (PMs)} has been developed by Takahashi et al.[20], Trezzolani et al.[21], and others[22,23]. Thrust force enhancement utilizing the higher magnetic flux density in the PM-type RF plasma thruster was experimentally tested by Takahashi et al., and higher thrust force by two times was successfully obtained by utilizing higher magnetic flux density by a factor of 2.5 [20]. On the other hand, utilization of the non-uniform magnetic field (convergence-divergence magnetic nozzle or magnetic cusp), which is located near the RF antenna, could improve the thrust performance[8,21,24]. In this helicon plasma source, the plasma production could be conducted more efficiently by utilizing the non-uniform magnetic field[24,25]. However, these surveys focused on the magnetic field strength and a magnetic field distribution has been performed individually, and the optimal configuration of the magnetic field has not been clarified since the magnetic field configuration complicatedly changes the plasma production and acceleration.

The thrust efficiencies of typical compact RF plasma thrusters are less than 10 %[20-22]. Due to the limitation of the performance of the magnetic material, performance improvement by utilizing the higher magnetic field with simple configuration is limited (the upper limit of the magnetic flux density in the 10 cm size thruster is about 0.1 T order in the case of the strongest magnetic material such as Nd-Fe-B[22,23]). In order to achieve a practical performance within a limited magnetic flux density, improvement of plasma production and acceleration by optimizing the magnetic field configuration is required.

In this study, the relation between the magnetic field configuration and thrust performance was investigated focusing on both of the plasma production and acceleration performance. Four types of PM-type RF plasma thrusters, which have different magnetic field distribution, were tested under the various operating conditions.

II. Design of PM-type RF Plasma Thruster

Design of our thruster is shown in Fig. 2. This thruster consists of the discharge vessel (Macor®), triple-loop type RF antenna (copper alloy), PMs (Nd-Fe-B), and magnetic yoke (steel alloy). The propellant gas was fed from a back plate of the thruster by a Pyrex® tube, and was ionized and exhausted by the RF power input and the static magnetic field, respectively. In this study, by changing the combination or arrangement of the PMs, four types of magnetic field distributions were constructed. The relationship between the intensity of the magnetic flux density and the thrust performance was investigated by two types of the thruster, in which only intensity of the magnetic flux density was different. The effect of non-uniformity of the magnetic field was examined by another two type thrusters, which had a magnetic cusp inside the discharge vessel: relative distance between the magnetic cusp and RF antenna was different between the two type thrusters.

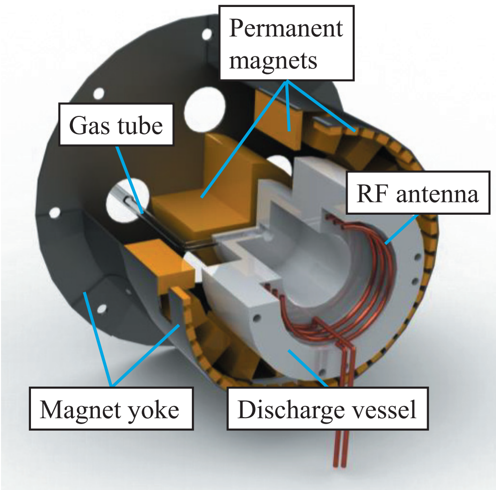

Figure 2. Schematic of PM-type RF plasma thruster.

A. Without Magnetic Cusp Model (RPT1 Series)

In the previous study of the RF plasma thruster with simple components, the improvement of the thrust performance by increasing the magnetic flux density was reported[20,22]. In this study, in order to investigate the effect of the magnetic flux intensity from view points of the thrust performance and the plasma production performance, two types of magnetic field were designed, as shown in Fig. 3. Both types of the RPT1-1 {Fig. 3 a)} and RPT1-2 {Fig. 3 b)} have almost the same magnetic flux distribution; magnetic field lines are parallel to the axis in the discharge vessel and abruptly divergent in the downstream of the thruster exit plane.

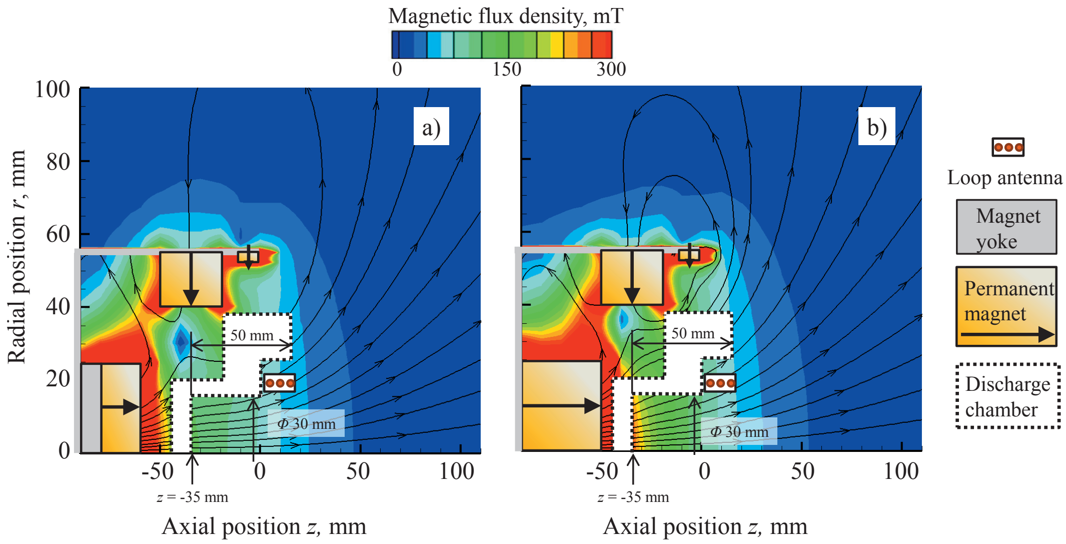

Figure 2. Magnetic flux density distributions in *r* - *z* plane of a) RPT1-1 and b) RPT1-2.

By changing the cylindrical magnet, the maximum magnetic flux density on the central axis of RPT1-2 (290 mT at the bottom end of the discharge vessel) is two times higher than that of the RPT1-1 (140 mT). The discharge vessel (I.D. 30 mm, 50 mm depth) and the RF antenna (triple-loop antenna at thruster exit) are put on same position in these two thrusters. The RF antenna is on the inside of the discharge vessel in order to ignite the plasma easily, and is electrically isolated to the plasma by the dielectric material.

B. With Magnetic Cusp Model (RPT2 Series)

In our previous study, the high-density plasma has been successfully produced in the presence of a magnetic cusp[26]. In order to produce the plasma more efficiently, two types of thrusters, which had magnetic cusps inside the discharge vessel, were constructed, as shown in Fig. 4. These thrusters have the same magnetic field; there are magnetic null (cusp) points in the center axis at the axial position z = -35 mm, and axial magnetic flux density is maximized (52 mT) at the axial position z = -10 mm. In these thrusters, positions of discharge vessels and RF antennas are different. In the RPT2-1 {Fig. 4 a)}, the center of the RF antenna is at magnetic cusp point and the end plate of the discharge vessel (I.D. 30 mm, 50 mm depth) is z = - 35 mm. On the other hand, the RF antenna and discharge vessel (I.D. 30 mm, 50 mm depth) of RPT2-2 {Fig. 4 b)} is shifted to the 30 mm upstream region, and the magnetic cusp of the RPT2-2 is in the middle area of the discharge vessel. Comparing the magnetic field to the one of RPT1 series, the intensity of magnetic flux density and the field distribution are different (Fig. 5). The magnetic field lines of RPT1 series are monotonically divergent type magnetic nozzle. On the other hand, RPT2-1 has a convergence-divergence magnetic nozzle, and RPT2-2 has very complex magnetic field lines (divergence and convergence-divergence magnetic nozzle). Summary of the characteristics of these thrusters focused on the magnetic field are shown in Table 1.

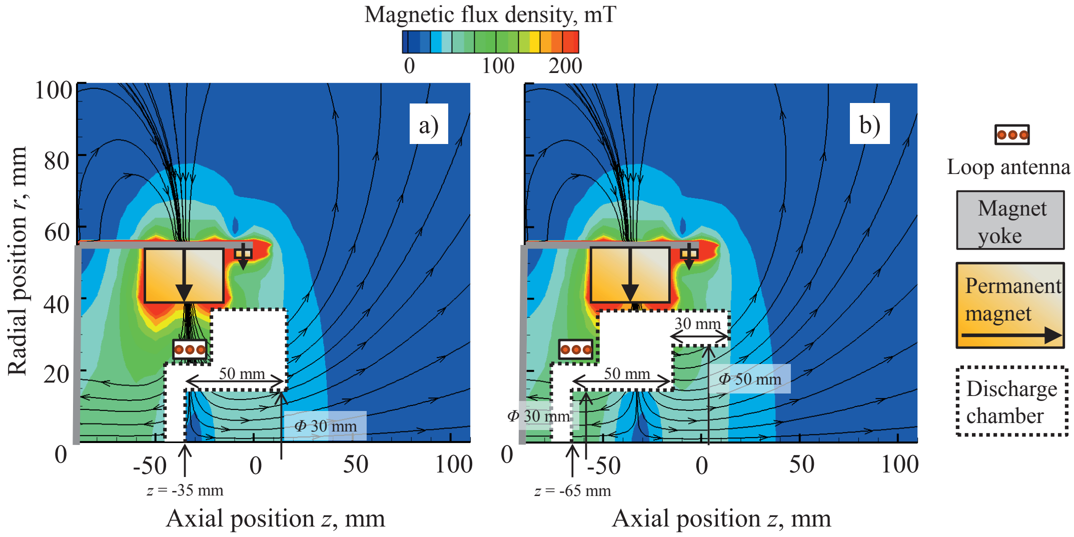

Figure 4. Magnetic flux density distributions in *r* - *z* plane of a) RPT2-1 and b) RPT2-2.

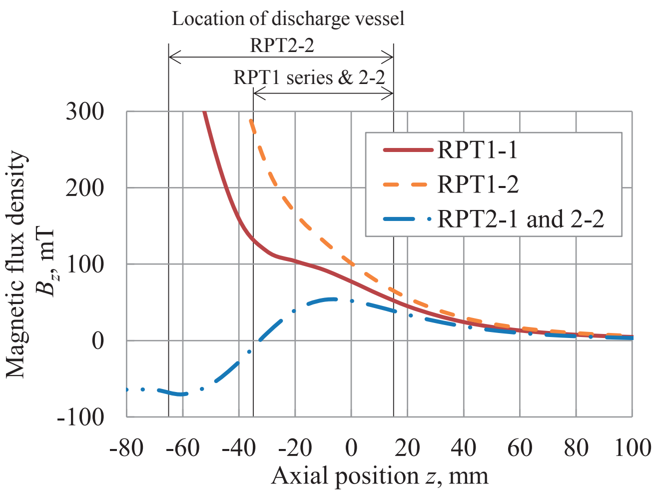

Figure 5. Axial distribution of axial magnetic flux density at *r* = 0 mm.

Table 1. List of thruster design parameters.

Thruster model	Position of magnetic cusp	Position of RF antenna	$B_{z,\,max}$
RPT1-1	Non-cusp	+ 10mm	140 mT at z = - 35 mm
RPT1-2	Non-cusp	+ 10 mm	290 mT at z = - 35 mm
RPT2-1	- 35 mm	- 35 mm	52 mT at z = - 10 mm
RPT2-2	- 35 mm	- 65 mm	52 mT at z = - 10 mm

III. Experiment

In this study, the thrust force measurement by the thrust stand and measurement of the total ion flux were conducted. The thrust performance (thrust force F, specific impulse I_{sp}, and thrust efficiency η_t) was estimated from the thrust measurement, and the propellant utilization efficiency η_u was from the total ion flux measurement.

A. Experimental Setup

Experimental setup for the thrust force and the total ion flux measurements of four types of PM-type RF plasma thrusters is shown in Fig. 6. These thrusters were installed within the vacuum chamber (I.D. 700 mm, 1,200 mm long). This chamber was evacuated by vacuum pumps (rotary pump × 3, diffusion pump × 1) down to 10^{-3} Pa or lower, and Ar gas was fed as a propellant by mass flow controller at a predetermined mass flow rate. When the RF pulse signal, which was manually triggered from the function generator (Tektronix AFG3022B), went to the RF power supply (Thamway T145-6326CK), an amplified RF pulse was transmitted to the RF antenna through a matching box (Thamway T020-5558A). Here, the RF signal frequency and a pulse width for plasma production were 13.56 MHz and 500 ms, respectively.

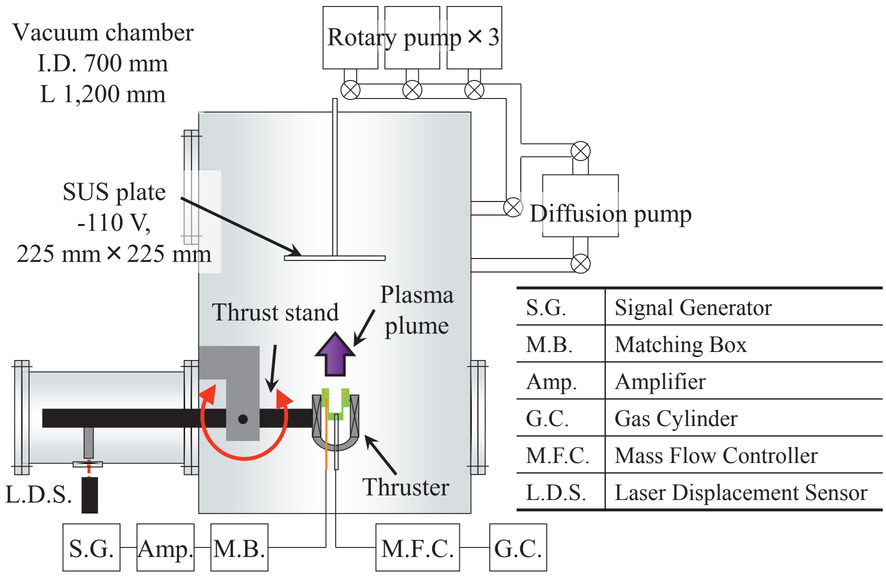

Figure 6. Experimental setup.

A torsion-pendulum type thrust stand was used for thrust measurement. In this study, the thruster components (the discharge vessel and the magnetic circuit) were mounted on the thrust stand. The RF antenna was mechanically isolated from the other components and thrust stand. This enables to measure the total thrust force, which is a summation of the thrust force components ($F = F_{diamag} + F_{thermal}$). The thrust force results in an arm displacement of the torsion-pendulum. This displacement was measured by a laser displacement sensor (KEYENCE, LK-G35A) with an accuracy of 0.5 μm. The relation between the thrust force and displacement was calibrated by applying repelling force using a samarium-cobalt bar magnet and an electromagnetic coil. For example, the sensitivity of this thrust stand in RPT1-1 was calibrated as $F \cdot \Delta t$ (μN·s) = $5.6 \cdot \delta$ (μm) ± 24 μN·s. This error was evaluated from the root mean square of the calibration unit accuracy (3 μN·s), an uncertainty of the laser displacement sensor (6 μN·s) and standard deviation from fitting line (23 μN·s).

For the ion flux measurement, -110 V biased SUS plate (225 mm × 225 mm) was located on 100 mm downstream from the thruster exit. This SUS plate collects all ions through a resistor (50 Ω) in a plasma plume except electrons. The size of SUS plate is enough large for a collection of the all plasma plume along the magnetic field lines from the thruster exit. Here, experimental condition is shown in Table 2.

Table 2. Experimental condition.

Vacuum pressure	1.6×10^{-1} Pa
Ar gas mass flow rate	1.2 mg/s
RF frequency for plasma production	13.56 MHz
RF power for plasma production	100 to 1000 W
RF pulse-width	500 ms

B. Experimental Results

From the measurements of the thrust force and the total ion flux, I_{sp}, η_t, and η_u were estimated using Eqs. (1), (2), and (3), respectively. In these estimations, the back flow from the vacuum chamber into the thruster discharge region (ingested mass flow) was taken into account. The effective mass flow rate from the thruster ($\dot{m}_{eff}$) was calculated as a summation of the injected mass flow rate $\dot{m}$ and the ingested one $\dot{m}_{ing}$, as shown in Eq. (4). $\dot{m}_{ing}$ was estimated using a pressure in the vacuum chamber P_c and area of the thruster exit A_e with assumed the neutral gas temperature T_n of room one (300 K). F, I_{sp}, η_t, and η_u are plotted in Figs. 7 and 8, as a function of the input RF power P_{source}. Here, P_{source} was defined as a subtraction of the reflection RF power from the forward one, whose two powers were measured by a directional coupler of the RF power supply. Error bars in Figs. 7 and 8 were derived from the standard deviation of multi-shot measurement. The thrust measurement of RPT2-2 is not plotted because its thrust force was lower than the resolution of thrust stand.

$$I_{sp} = \frac{F}{g_0 \dot{m}_{eff}}, \tag{1}$$

$$\eta_t = \frac{F^2}{2\dot{m}_{eff} P_{source}}, \tag{2}$$

$$\eta_u = \frac{I_{i,sat}}{e\frac{\dot{m}}{m_n}}, \tag{3}$$

$$\dot{m}_{eff} = \dot{m} + \dot{m}_{ing} = \dot{m} + \frac{1}{4} A_e P_c \sqrt{\frac{m_n}{k_B T_n}}. \tag{4}$$

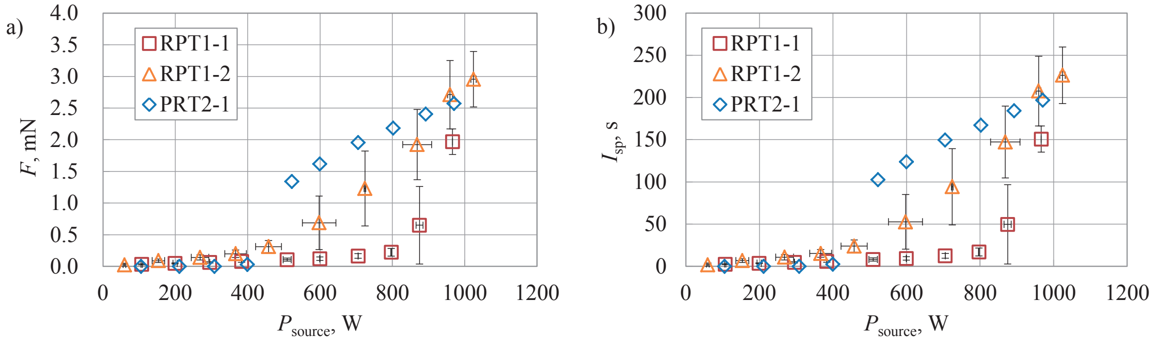

Figure 7. Thrust performance vs RF power input; a) thrust force and b) specific impulse.

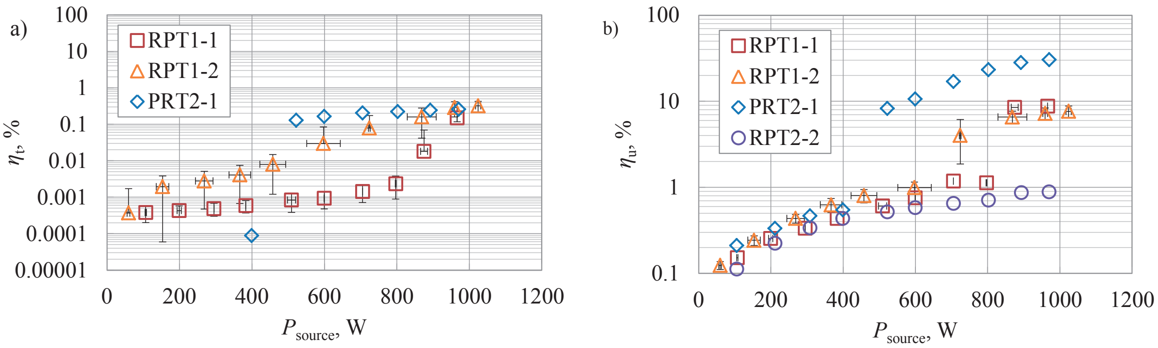

Figure 8. Efficiency vs RF power input; a) thrust efficiency and b) propellant utilization efficiency.

From Figs. 7 and 8, thrust performance (F, I_{sp}, and η_t) and η_u monotonically increased with P_{source} in all type thrusters (RPT1-1, 1-2, and 2-1). In addition, there were critical operating points, in which the thrust performance was rapidly improved by increment of P_{source}. In these critical operating points, η_u was also improved {Fig. 8 b)}. This improvement indicates an increment of total flux of the plasma plume. The density jump was reported in the RF plasma generation[12,13,26]; the discharge mode transition from the capacitively coupled plasma (CCP) to the inductively coupled plasma (ICP) or from ICP to the helicon mode plasma. Generally, the plasma production efficiency of ICP (helicon) mode discharge is higher than that of CCP (ICP) mode discharge. Therefore, thrust performance was improved by the increment of the plasma flux in the magnetic nozzle. P_{source} at this critical operating point was related to the magnetic field configuration and position of the RF antenna; 900-1,000 W in RPT1-1, 600-700 W in RPT1-2, and 400-500 W in RPT2-1 (RPT2-2 was not observed). η_u before the discharge mode transition was comparable in each type thruster. On the other hand, after the transition, this efficiency of the RPT2-1 became more than twice higher than those of RPT1-1 and RPT1-2 with the same P_{source}. These results show that RPT2-1 has the higher plasma production performance than other type thrusters. Focusing on the thrust performance, the highest F and η_t of 3.0 mN, 0.32 % was obtained by RPT1-2 at P_{source} of 1,000 W. Since η_u of RPT1-2 (7.6 % at 1,000 W) was much lower than the one of RPT2-1 (30 % at 970 W), plasma plume in RPT1-2 was accelerated more efficiently by the higher magnetic flux density.

IV. Discussion for Improvement of the Thrust Performance

In order to consider the relation between the thrust performance and the plasma production performance, η_t is plotted against η_u in Fig. 9. η_t was improved by increasing η_u in all type thrusters. In this experiment, higher η_u was obtained in RPT2-1, which has a magnetic cusp at the center of the RF antenna. In the case of same η_u (i.e., the case same plasma flux), the thrust efficiency of RPT1-2, which has a high magnetic flux density, was higher than the other type thrusters. From Fig. 9, it is indicated that the following thruster conditions are effective to improve η_t: a discharge mode after the transition by an increment of P_{source}, for transit the discharge mode, high magnetic flux density leading to the effective plasma acceleration, and a magnetic cusp leading to the improvement of the plasma production. Note that, the plasma production performance of the RPT2-2, which has a magnetic cusp positioned downstream of the RF antenna, became lower than no magnetic cusp type thruster. Therefore, more detailed investigation of the utilization of the magnetic cusp (position and intensity of the magnetic nozzle) in the RF plasma thruster must be conducted in our future works.

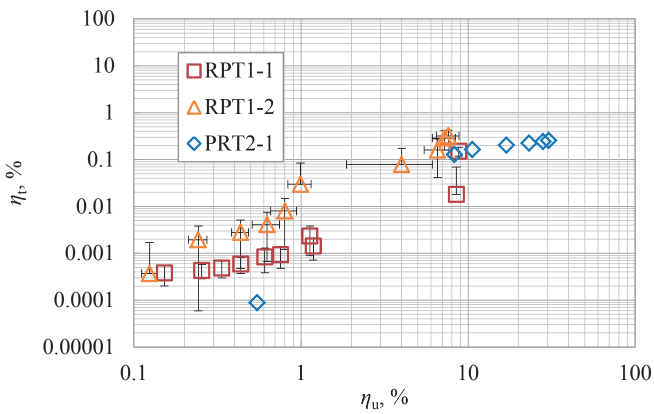

Figure 9. Thrust characteristics.

V. Conclusion

The relation between the thrust performance and plasma production one was investigated using PM-type RF plasma thrusters varying the magnetic field configuration. From the measurements of the thrust force and the total ion flux, η_t monotonically increased with η_u. Discharge mode transition from the CCP (ICP) to the ICP (helicon) improved η_u by increasing P_{source}. The critical operating point of the discharge mode transition was related to the magnetic field configuration; the case with magnetic cusp at the center of the RF antenna led to a high performance discharge mode with the lower RF power than no magnetic cusp case. Finally, η_t of 0.15, 0.32, and 0.26 % in P_{source} of 1 kW was obtained by RPT1-1 (140 mT without magnetic cusp), PRT1-2 (290 mT without magnetic cusp), and RPT2-1 (52 mT with magnetic cusp at center of RF antenna), respectively.

By comparing the performances of RPT1-1, RPT1-2, and RPT2-1, the relationship between the thrust performance and magnetic field configuration was examined. When the plasma flux was the same, the highest η_t was obtained by RPT1-2, which has high magnetic flux density for the magnetic nozzle up to 290 mT, and this efficiency was more than two times higher than that of RPT1-1, which has 140 mT for the magnetic nozzle. On the other hand, in the same P_{source} case of 1 kW, η_t of RPT2-1, which has a magnetic cusp at the center of the RF antenna, was comparable to that of RPT1-2, even though the magnetic flux density of RPT2-1 was more than 5 times lower than that of RPT1-2.

References

[1]Chang Díaz, F. R., "The VASIMR Rocket," *Sci. American*, Vol. 283, Nov. 2000, pp. 90-97.

[2]Squire, J. P., Cassady, L. D., Chang Díaz, F. R., Carter, M. D., Glover, T. G., and Ilin, A. V., et al., "Superconducting 200 kW VASIMR® Experiment and Integrated Testing," *31st Int. Electric Propul. Conf.*, IEPC-2009-209, Michigan, 20-24 Sept., 2009.

[3]Cassady, L. D., Longmier, B. W., Olsen, C. S., Ballenger, M. G., McCaskill, G. E., Ilin, A. V, et al., "VASIMR® Performance Results," *46th AIAA/ASME/SAE/ASEE Joint Propul. Conf. & Exhibit*, AIAA 2010-6772, Nashville, 25-28 July, 2010.

[4]Charles, C., and Boswell, R. W., "Current-free Double Layer Formation in a High-density Helicon Discharge," *Appl. Phys. Lett.*, Vol. 82, No. 9, 2003, pp. 1356-1358.

[5]Musso, I., Manente, M., Carlsson, J., Giacomuzzo, C., Pavarin, D., Angrilli, F., et al., "2D OOPIC Simulations of the Helicon Double Layer Thruster," *30th Int. Electric Propul. Conf.*, IEPC-2007-146, Florence, 17-20 Sept., 2007.

[6]West, M. D., Charles, C., and Boswell, R. D., "Testing a Helicon Double Layer Thruster Immersed in a Space-Simulation Chamber," *J. Propul. Power*, Vol. 24, No. 1, 2008, pp. 134-141.

[7]Takahashi, K., Lafleur, T., Charles, C., Alexander, P., Boswell, R. W., Perren, M., et al., "Direct Thrust Measurement of a Permanent Magnet Helicon Double Layer Thruster," *Appl. Phys. Lett.*, Vol. 98, No. 14, 2011, pp. 141503 1-3.

[8]Takahashi, K., Lafleur, T., Charles, C., Alexander, P., and Boswell, R. W., "Electron Diamagnetic Effect on Axial Force in an Expanding Plasma: Experiments and Theory," *Phys. Rev. Lett.*, Vol. 107, No. 23, 2011, pp. 23501 1-4.

[9]Takahashi, K., Charles, C., and Boswell, R. W., "Approaching the Theoretical Limit of Diamagnetic-Induced Momentum in a Rapidly Diverging Magnetic Nozzle," *Phys. Rev. Lett.*, Vol. 110, No. 19, 2013, pp. 195003 1-5.

[10]Willianms, L. T., and Walker, M. L. R., "Thrust Measurements of a Radio Frequency Plasma Source," *J. Propul. Power*, Vol. 29, No. 3, 2013, pp. 520-527.

[11]Toki, K., Shinohara, S., Tanikawa, T., and Shamrai, K. P., "Small Helicon Plasma Source for Electric Propulsion," *Thin Solid Films*, Vol. 506-507, 2006, pp. 597-600.

[12]Shinohara, S., Hada, T., Motomura, T., Tanaka, K., Tanikawa, T., Toki, K., et al., "Development of High-density Helicon Plasma Sources and Their Applications[a]," *Phys. Plasmas*, Vol. 16, No. 5, 2009, pp. 057104 1-10.

[13]Shinohara, S., Nishida, H., Tanikawa, T., Hada, T., Funaki, I., and Shamrai, K. P., "Development of Electrodeless Plasma Thrusters with High-Density Helicon Plasma Source," *IEEE Trans. Plasma Sci.*, Vol. 42, No. 5, 2014, pp. 1245-1254.

[14]Batishchev, O. V., "Minihelicon Plasma Thruster," *IEEE Trans. Plasma Sci.*, Vol. 37, No. 8, 2009, pp. 1563-1571.

[15]Kuwahara, D., Mishio, A., Nakagawa, T., and Shinohara, S., "Development of Very Small-Diameter, Inductively Coupled Magnetized Plasma Device," *Rev. Sci. Instrum.*, Vol. 84, No. 10, 2013, pp. 103502 1-4.

[16]Fruchtman, A., "Electric Field in a Double Layer and the Imparted Momentum," *Phys. Rev. Lett.*, Vol. 17, No. 6, 2006, pp. 065002 1-4.

[17]Ahedo, E, and Merino, M., "Two-dimensional Supersonic Plasma Acceleration in a Magnetic Nozzle," *Phys. Plasmas*, Vol. 17, No. 7, 2010, pp. 073501 1-15.

[18]Longmier, B. W., Bering III, E. A., Carter, M. D., Cassady, L. D., Chancery, W. J., Chang Díaz, F. R., et al., "Ambipolar Ion Acceleration in an Expanding Magnetic Nozzle," *Plasma Sources Sci. Tech.*, Vol. 20, No. 1, 2011, pp. 015007 1-9.

[19]Squire, J. P., Olsen, C. S., Franklin, R., Díaz, C., Cassedy, L. D., Longmier, B. W., et al., "VASIMR® VX-200 Operation at 200 kW and Plume Measurement: Future Plans and ISS EP Test Platform," *32nd Int. Electric Propul. Conf.*, IEPC-2011-154, Wiesbaden, 11-15 Sept., 2011.

[20]Takahashi, K., Charles, C., Boswell, R. B., and Ando, A., "Performance Improvement of a Permanent Magnet Helicon Plasma Thruster," *J. Phys. D: Appl. Phys.*, Vol. 46, No. 35, 2013, pp. 352001 1-5.

[21]Trezzolani, F., Fabris, A. L., Pavarin, D., Selmo, A., Tsaglov, A. I., Loyan, A. V., et al., "Low Power Radio-Frequency Plasma Thruster Development and Testing," *33rd Int. Electric Propul. Conf.*, IEPC-2013-153, Washington, 6-10 Oct., 2013.

[22]Nakamura, T., Ito, S., Nishida, H., and Shinohara, S., "Thrust Performance of High Magnetic Field Permanent Magnet Type Helicon Plasma Thruster," *50th AIAA/ASME/SAE/ASEE Joint Propul. Conf.*, AIAA 2014-3474, Cleveland, 28-30 July, 2014.

[23]Otsuka, S., Nakagawa, T., Ishii, H., Teshigahara, N., Fujitsuka, H., Waseda, S., et al., "Generation and Acceleration of High-Density Plasma Using Permanent Magnets for the Completely Electrodeless Propulsion System," *Plasma Fus. Res.*, Vol. 9, 2014, pp. 3406047 1-5.

[24]Shamrai, K. P., Shinohara, S., Virko, V. F., Slobodyan, V. M., Virko, Y. V., and Kirichenko, G. S., "Wave Stimulated Phenomena in Inductively Coupled Magnetized Plasmas," *Plasma Phys. Control. Fusion*, Vol. 47, No. 5A, 2005, pp. A307-A315.

[25]Chevalier, F., and Chen, F. F., "Experimental Modeling of Inductive Discharges," *J. Vac. Sci. Tech. A.*, Vol. 11, No. 4, 1993, pp. 1165-1171.

[26]Nakamura, T., Nishida, H., Shinohara, S., Funaki, I., Tanikawa T., and Hada, T., "Preliminary Investigation of Electromagnetic Thrust Characteristics in Electrodeless Compact Helicon Plasma Thruster," *Trans. JSASS Aerospace Tech. Japan*, Vol. 12, No. ists29, 2014, pp. Po_1_1-Po_1_6.